

## Accepted Manuscript

Title: Antifungal Graphene Oxide-Borneol Composite

Authors: Guofeng Li, Hongjuan Zhao, Jie Hong, Kecheng Quan, Qipeng Yuan, Xing Wang

PII: S0927-7765(17)30601-X  
DOI: <http://dx.doi.org/10.1016/j.colsurfb.2017.09.023>  
Reference: COLSUB 8842

To appear in: *Colloids and Surfaces B: Biointerfaces*

Received date: 7-6-2017  
Revised date: 12-8-2017  
Accepted date: 9-9-2017



Please cite this article as: Guofeng Li, Hongjuan Zhao, Jie Hong, Kecheng Quan, Qipeng Yuan, Xing Wang, Antifungal Graphene Oxide-Borneol Composite, *Colloids and Surfaces B: Biointerfaces* <http://dx.doi.org/10.1016/j.colsurfb.2017.09.023>

This is a PDF file of an unedited manuscript that has been accepted for publication. As a service to our customers we are providing this early version of the manuscript. The manuscript will undergo copyediting, typesetting, and review of the resulting proof before it is published in its final form. Please note that during the production process errors may be discovered which could affect the content, and all legal disclaimers that apply to the journal pertain.

## Antifungal Graphene Oxide-Borneol Composite

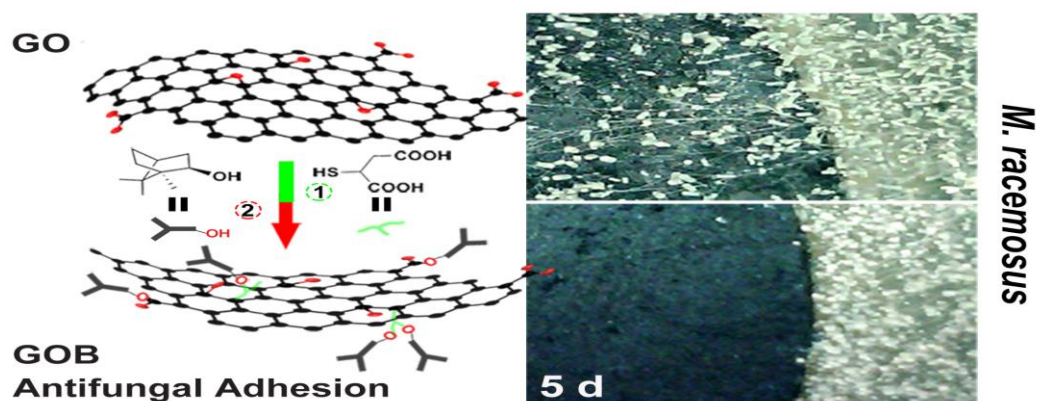
Guofeng Li, Hongjuan Zhao, Jie Hong, Kecheng Quan, Qipeng Yuan, Xing Wang\*

The State Key Laboratory of Chemical Resource Engineering, Beijing Laboratory of Biomedical Materials, Beijing University of Chemical Technology, Beijing 100029, P. R. China

\*Corresponding author. Tel: 86 10-64416428 E-mail address:

wangxing@mail.buct.edu.cn (X. W.)

### GRAPHICAL ABSTRACT



### Highlights

- Graphene oxide-borneol (GOB) composite is a novel antifungal material.
- GOB against adhesion and growth of *M. racemosus* on its surface for a long-term.
- Carbon stereochemistry plays a crucial role on antifungal properties rather than hydrophobicity.
- GOB is biocompatible material.
- Landing experiment and sensing mechanism are proposed in this work.

**ABSTRACT:** Although antibacterial activities of graphene oxide (GO) and its derivatives have been investigated comprehensively, their antifungal properties are still less reported. Yet, fungal contamination seriously threatens the public health. Herein, we present a design of graphene oxide-borneol (GOB) composite, and report its great antifungal effect. This GOB composite is prepared by esterification of borneol with thiomalic-acid-modified GO sheets, where the linker molecule is used to increase surface carboxyl groups. As a result, the antifungal activity displays a dramatically conversion from no activity of GO and its derivatives to distinct antifungal adhesion and growth inhibition of the GOB. Under microscopy, few spores can be found on the GOB surface, while large numbers of sporangia and spores adhere and grow on the control groups. It is also worth noting that on the GOB sample the fallen spore does not germinate even after 5 days, demonstrating a long-term antifungal effect of the GOB composite. Further studies confirm that carbon stereochemistry rather than wettability plays a crucial role on the antifungal adhesion properties. This study not only highlights a promising GOB composite as a candidate of graphene-based antifungal agent, but also provides us with in-depth understanding of the interactions between fungi and graphene-based materials.

**KEYWORDS:** antifungal activity, graphene oxide, borneol, composite, stereochemistry

## 1. Introduction

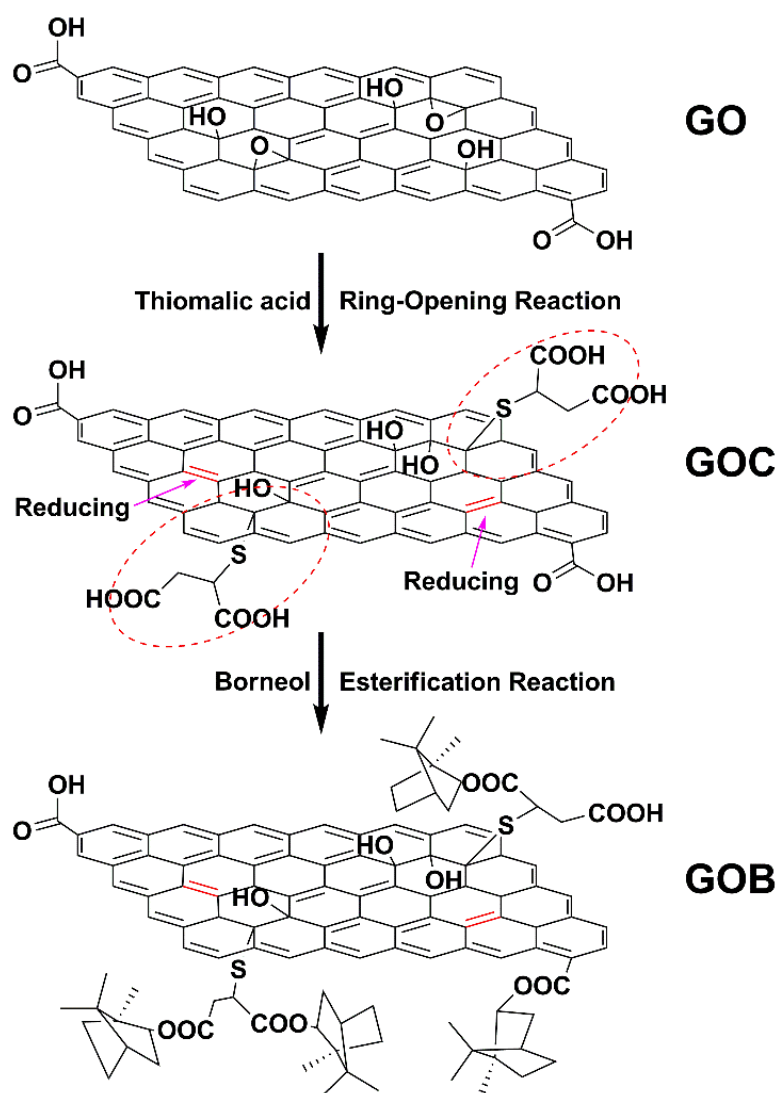
Fungi can easily colonize on the surfaces of most materials and rapidly spread fungal spores [1]. The formation of fungal contamination seriously threatens human health and may cause huge economic losses [2–5]. Therefore, effective method against those organism is highly desired. One kind of the most recently developed biocidal nanomaterials is graphene and its derivatives [6–14]. They are intensively studied as carbon-based antimicrobial materials with many potential applications, such as use in the field of medicine, energy and environment [6,15,16]. As a breakthrough, Hu *et al* found that metabolic activity of *E. coli* decreases dramatically in the presence of GO or reduced GO (RGO) sheets [17]. Liu *et al* revealed that GO derivative could aggregate and locally damage the cell membrane integrity [18]. Tu *et al* made a deeper insight that graphene and GO destruct and extract the phospholipids of *E. coli* membranes [19]. A comprehensive understanding was reported by Hui *et al*, they demonstrated the key influence factor of proteins on realizing their antibacterial effects. Presence of proteins can inhibit the antibacterial properties of graphene-based materials (GMs) [20]. However, until now, most of the antimicrobial studies of GMs mainly focus on antibacterial performance, rather than antifungal property [21–25]. This situation is also in agreement with other antimicrobial materials. More than 90% of the researches are about antibacterial materials, while antifungal materials are less than 10% [26–29].

Recently, the GO-silver nanocomposite with antifungal performance was reported [30], in which the silver nanoparticles wrapped into graphene nanoscrolls exhibit ideal lengthened activities by durative slow-releasing. Han's group revealed that GO-silver nanocomposite obtained by electrostatic self-assembly can also be a novel antifungal agent for crop disease prevention [31]. Besides, Chen *et al* indicated the antimicrobial activity of GO can be triggered in liquid system, where it can interwind bacteria and fungal spores, resulting in membrane damage of the cells [32]. These studies suggest that the GMs are potential antifungal materials. To achieve superior antifungal performance, two aspects should be taken into account. On the one hand, the use of silver nanoparticles should be cautious. Silver nanoparticles have been demonstrated to cause adverse effects for organism and, especially, humans [33–35]. On the other hand, antifungal performance on the solid surfaces of the GMs is needed. Filamentous fungi grow on solid surfaces can penetrate progressively deeper into the substrate [36,37]. Studies showed that surface contamination in hospital is heavy and threaten patients' lives [38]. Improving antifungal performance of the GMs on solid surface is still a challenge. Therefore, a new strategy is required to enhance the antifungal effect of the GMs on solid surface, meanwhile, ensure its biosafety.

Previous studies demonstrate that chiral biointerface has great influence on cells adhesion and proteins adsorption [39–43], which inspired us to further develop antimicrobial materials or surfaces by taking advantage of the “chiral taste” of microbes. L-borneol is a hydrophobic bicyclic monoterpene [44], and widely used as a

safe and natural medical molecule [45]. Recently, our group revealed that borneol-based polymers [46,47] or borneol-grafted cellulose [48] have unique antimicrobial adhesion properties by dramatically reducing microbial attachment and biofilm formation. Thus, we deduced that borneol-grafting was an effective strategy for endowing antifungal activity to solid graphene.

Herein, we present a GO-borneol (denote as GOB) composite synthesized by esterification of borneol with thiomalic-acid-modified GO sheets, of which thiomalic acid is used as the linker molecule to increase surface carboxyl groups (Scheme 1). The covalent banding between GO and borneol prevents the shedding of borneol and gives a long-term antifungal effect to the GOB composite. With this modification, both antifungal activity and cytotoxicity of the GOB could be optimized compared with those of GMs, thus suggesting the GOB is a promising antifungal composite.



**Scheme 1.** Schematic representation of the fabricate processes of the GOB composite.

Thiomalic acid is used as the linker to increase surface carboxyl groups by opening of epoxy ring reaction. The linkers modified GO sheet is denoted as the GOC. Partial reducing happens within this reaction according to the characterizations. After esterification with borneol molecules, the resulted GOB composite is obtained.

## 2. Experimental

## 2.1. Materials

Graphite powder (80 mesh) was purchased from Qingdao Jinrilai Co., Ltd., Shandong, China. L-borneol (97%), thiomalic acid (98%) and 4-methylbenzenesulfonic acid (95%) was purchased from J&K Scientific Ltd. 3-(4,5-dimethyldiazol-2-yl)-2,5-diphenyl tetrazolium bromide (MTT) was purchased from Simcere, Jiangsu, China. Sulfuric acid ( $\text{H}_2\text{SO}_4$ , 98%), potassium permanganate ( $\text{KMnO}_4$ , 99.9%), sodium nitrate ( $\text{NaNO}_3$ , AR), hydrochloric acid ( $\text{HCl}$ , 37%) and hydrogen peroxide ( $\text{H}_2\text{O}_2$ , 30%), N,N-dimethylformamide (DMF, 99%), triethylamine (TEA, 99%), hydrazine hydrate (98%) and other general reagents were purchased from Sinopharm Chemical Reagent Co., Ltd. L-929 mouse fibroblast cells were supported by the Key Laboratory of Bioorganic Phosphorus Chemistry & Chemical Biology, Tsinghua University.

## 2.2. Preparation of GO

Graphite powder (4 g) and sodium nitrate (2 g) were dispersed into 80 mL sulfuric acid (98%) and stirred at 0 °C. Potassium permanganate (12 g) was slowly added and stirred at 0 °C for other 10 min. Then, the solution was kept at 37 °C for 4 h. After adding 150 mL water, the mixture was maintained at 98 °C for 30 min. Then, the reaction was stopped by added 200 mL water. About 15 mL hydrogen peroxide (30%) was added gradually until the mixture turned yellow. After washing with water sufficiently, a GO solution ( $5 \text{ mg mL}^{-1}$ ) was obtained by ultrasonic exfoliation and centrifugation [49,50].

## 2.3. Preparation of the GOB

GO (0.1 g) was dissolved in 20 mL of anhydrous DMF by sonication. Thiomalic acid (0.2 g) was added to above GO solution at 40 °C. After adding 3 mL of TEA under vigorous stirring, the mixture was allowed to react for 48 h. The product was filtrated, washed and dialyzed with water. After lyophilization, the GOC was obtained. The obtained GOC was dissolved in 20 mL anhydrous DMF. About 1 g of L-Borneol and 0.2 g of 4-methylbenzenesulfonic acid (catalyst) were added. After vigorous stirring for 12 h at 70 °C, the resulting material GOB was yield and purified by water dialyzed.

#### **2.4. Characterization of the GOB**

Water contact angle (WCA) of the GOB was measured on a Dataphysics OCA20 at room temperature. De-ionized water was used here. Energy-dispersive spectrometry (EDS, Hitachi S-4700) and fourier transform infrared spectroscopy (FTIR, Nicolet-20DXB) were used to analysis the chemical composition of the GOB. X-ray diffraction (XRD, D/Max 2500 VB2+/PC) and Raman spectroscopy (RENISHAW inWia) were used to analysis the structure of the GOB.

#### **2.5. Antifungal Activity Test**

Antifungal activity assay was carried out according to the reported method [48]. The powder of GO, RGO, GOC and the GOB were pressed into 13 mm diameter sized pellets (thickness=1 mm), and they were individually affixed onto the beef extract peptone solid medium. Then, 10  $\mu$ L *Mucor racemosus* (*M. racemosus*) suspension was dropped in the center of the plate and was aerobically cultured at 37 °C. The fungi were

allowed to grow and expand from the medium center to the pellet surface. After 120 h incubation, fungal growth was observed and recorded with a camera. The morphologies of fungal cells on the sample surface were observed using a Hitachi S-4700 scanning electron microscopy (SEM). Before SEM observation, the fungal cells were immobilized and dehydrated through 2.5% glutaraldehyde and gradient ethanol (50, 60, 70, 80, 90 and 100%), respectively [48].

## 2.6. Cytotoxicity Evaluation

MTT assay was used to evaluate the cytotoxicity of the synthetic GO, RGO, the GOC and the GOB. Briefly, the MTT test was performed based on the European standard EN ISO10993-5:2003. Firstly, L929 mouse fibroblast cells were propagated in Roswell Park Memorial Institute (RPMI) 1640 medium supplemented with 10% fetal bovine serum (FBS), 100 units  $\text{mL}^{-1}$  penicillin and 100  $\mu\text{g mL}^{-1}$  streptomycin at 37 °C in a humidified condition of 95% air and 5%  $\text{CO}_2$ . L929 cells in logarithmic growth-phase were collected and seeded in 96-well plate ( $8 \times 10^4$  cells per well) for 24 h. Simultaneously, the four material tablets (diameter=1.1 cm, double side) were ultraviolet sterilized and infused in 2 mL RPMI 1640 medium for 24 h. Then, those impregnating solutions were used as the complete cell culture medium, by adding 10% FBS, 100 units  $\text{mL}^{-1}$  penicillin and 100  $\mu\text{g mL}^{-1}$  streptomycin generally. After removing the culture medium from above mentioned 96-well plate, the impregnating solution was used as new culture medium (100  $\mu\text{L}$ ) at the same conditions for another 48 h. Thirdly, an MTT assay was performed by adding 20  $\mu\text{L}$  MTT working solution

(5 mg mL<sup>-1</sup>) to each well and then cells were incubated for another 4 h. After that, culture medium was replaced with 150  $\mu$ L DMSO. Lastly, the absorbance of the solution was measured by ThermoMax Microplate Reader at 490 nm, and the value of relative growth rate (RGR) was calculated according to the formula as follows: RGR (%) =  $\text{Abs}_{490 \text{ sample}} / \text{Abs}_{490 \text{ control}} \times 100$ . Finally, the toxicity grade of each material was assessed.

### **3. Results and Discussions**

#### **3.1. Material Characterization**

The GOB was obtained through two steps of surface grafting (Scheme 1). At the first step, thiomalic acid is used as the linker to increase the surface carboxyl groups of GO. Although GO contains large numbers of oxygen functional groups, the carboxyl groups are limited and mainly concentrate on the edge of GO nanosheets [51,52]. These small amount of carboxyl groups limits the grafting of borneol. Therefore, thiomalic acid was used to effectively increase the amount of carboxyl groups on GO surface. Moreover, when borneol was modified by esterification with carboxyl groups, the linker is in favor of improving the distribution of borneol on the surface of GO nanosheet.

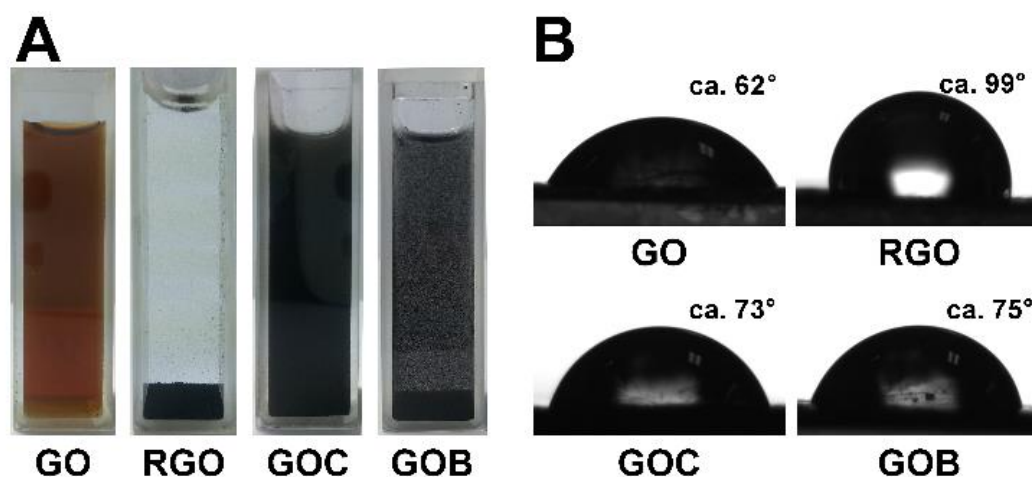


**Fig. 1.** (A) The optical images of the water dispersion of GO, RGO, the GOC and the GOB. (B) The WCA of GO, RGO, the GOC and the GOB. Data are mean  $\pm$  standard deviation ( $n = 5$ ).

Because the grafting functional groups were different, the aqueous dispersion was variation during this process. As shown in Fig. 1A, GO with abundant oxygen functional groups can evenly disperse in water. While after a general reduction reaction, the obtained RGO is hydrophobic and aggregates at the bottom of disk. Water contact angle (WCA) of RGO changes to  $99^\circ$  from the original  $62^\circ$  of GO (Fig. 1B). When grafting thiomalic acid to GO through click reaction, GO is reduced in a certain extent [53], and the obtained GOC could be a stable but black solution. As the grafted thiomalic acid is hydrophilic, the water dispersion of the GOC is greatly enhance comparing with that of RGO (Fig. 1A). The WCA of the GOC is about  $70^\circ$  (Fig. 1B). Borneol is a hydrophobic bicyclic monoterpene. When borneol grafted onto the GOC, the carboxyl in the GOC was replaced by borneol-ester. Thus, the obtained GOB

aggregates again (Fig. 1A). Black particles are visible, and most of the GOB particles precipitate at the bottom. The WAC of the GOB tablet increased to 75° (Fig. 1B). These phenomena indicated that borneol was successfully grafted to GO.

FTIR spectra was conducted to further verify the GOB composite (Fig. 2A). In the spectra, a broad O–H stretching peak is observed at 3397  $\text{cm}^{-1}$  for GO, whereas this peak in the GOC or the GOB is shrunk as well as in RGO. Besides, the aromatic C=C stretching peaks (1558  $\text{cm}^{-1}$ ) in the GOC and the GOB become apparent. These phenomena were in an agreement with the aforementioned results that the GOC and the GOB are partially reduced during the grafting process. After the modification of GO with thiomalic acid, the relative intensity of the epoxy C–O stretch (1044  $\text{cm}^{-1}$ ) of the GOC significantly decreased, suggesting that thiomalic acid has been grafted on graphene by ring opening reaction [54]. In the case of the GOB, the peak of ester (C–O at 1175  $\text{cm}^{-1}$ ) is greatly enhanced. Simultaneously, the  $\text{sp}^3$  and  $\text{sp}^2$  C–H stretch of borneol at 2922 and 2855  $\text{cm}^{-1}$  are distinct. These results further revealed that borneol has grafted on GO successfully.

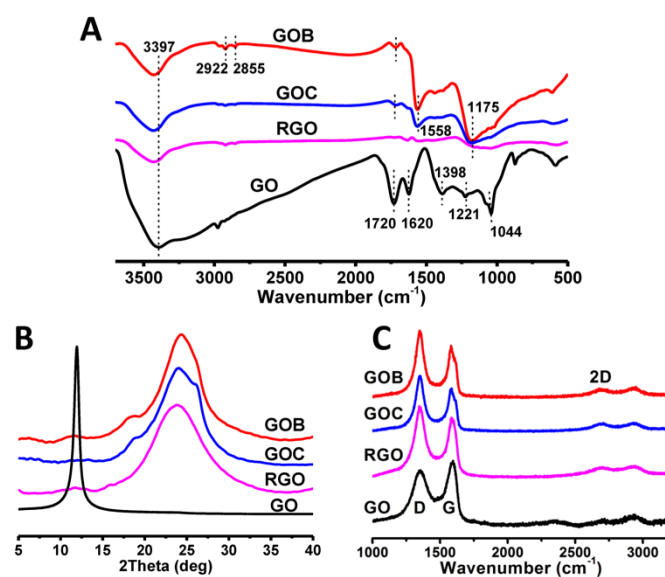


**Fig. 2.** (A) FTIR, (B) XRD and (C) Raman analyses of GO, RGO, the GOC and the GOB.

The grafting borneol can result in the change of structure of the GOB. Thus, it was characterized by XRD and Raman spectra. In Fig. 2B, GO has a typical diffraction peak at  $2\theta=12^\circ$ . When carboxyl acid or borneol is grafted to GO, the diffraction peak is broad and centered at  $2\theta=25^\circ$  ( $d=0.35$  nm). This peak is similar with RGO, suggesting that the reducing property of the grafting process. But, there is a new emerge peak at  $2\theta=18.5^\circ$  ( $d=0.48$  nm) in the GOC when compared with RGO. This is mainly due to the presence of carboxyl acid groups, which increased the d-space between graphene sheets. Consistent with this surmise, the diffraction peak at  $2\theta=18.5^\circ$  notably increases in the GOB because borneol is a cage structure that its steric hindrance further increases the d-space of the GOC. Raman spectra (Fig. 2C) shows that they have similar Raman

peaks that the G peak is around  $1593\text{ cm}^{-1}$  and the D peak is around  $1358\text{ cm}^{-1}$ . The D peak and the G peak represent the structural defects and the first-order scattering of the  $E_{2g}$  mode, respectively [55]. The integral area ratio (ID/IG) of GO is about 1.27, while that of RGO increases to 1.65 because of the disordered structure caused by reduction reaction. The linkers can slightly reduce GO, so the ID/IG ratio of the obtained GOC is up to 1.46. Borneol's introduction can further destroy the structure. The GOB has more defects, and the ID/IG ratio is about 1.51. The 2D band of the GOB is located at about  $2695\text{ cm}^{-1}$ , and the 2D/G ratios is 0.24. According to the previous study [56], the GOB is multi-layer graphene sheets. These results implied that the GOB surface had many structural defects capped with borneol groups.

EDS characterizations (Fig. 3) show a distinct difference for the element content of the GOB when compared with that of GO. Apparently in an equal area, the distribution of C element and S elements in the GOB are observably increased, while the distribution of O is less than that in the GO, indicating that borneol is uniformly distributed on the surface of graphene. Specifically, the amount of S is increased to 1.6 wt% from 0.7 wt% of the original GO (Table 1), suggesting that the linker of thiomalic acid is grafted. According to the content of S element in thiomalic acid, we can calculate that the grafting linkers on GO are about 5.1 wt%. Deducting the amount of C element (1.4 wt%) in the linker, there are about 18.5 wt% of C element increased by the grafted borneol. The grafting rate, therefore, could be calculated that approximately 23.8 wt% of borneol was grafted on the GOB.

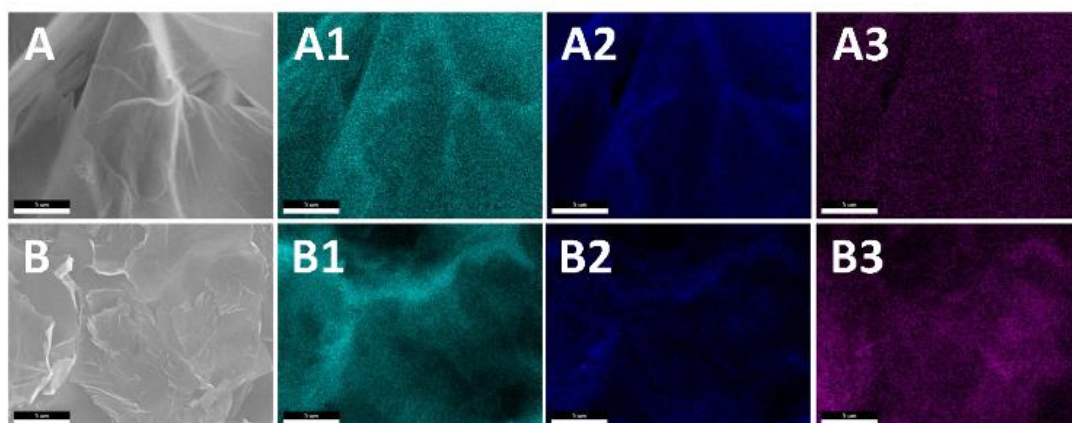


**Fig. 3.** (A) SEM image of GO and the corresponding EDS mapping of (A1) C, (A2) O and (A3) S elements. (B) SEM image of the GOB and the corresponding EDS mapping of (B1) C, (B2) O and (B3) S elements. The scale bar is 5  $\mu\text{m}$ .

**Table 1.** The elements compose of GO and the GOB<sup>a</sup>.

	<b>C (wt%)</b>			<b>O (wt%)</b>	<b>S (wt%)</b>		
	<i>GO</i>	<i>linker</i>	<i>borneol</i>		<i>GO</i>	<i>linker</i>	<i>borneol</i>
<b>GO</b>	<b>60.9</b>			<b>38.5</b>	<b>0.7</b>		
	<i>60.9</i>	--	--		<i>0.7</i>	--	--
<b>GOB</b>	<b>80.8</b>			<b>17.6</b>	<b>1.6</b>		
	<i>60.9</i>	<i>1.4</i>	<i>18.5</i>		<i>0.7</i>	<i>0.9</i>	--

<sup>a</sup> The bold and the italic numbers represent the total and the subunit contents (wt%), respectively. Linker represents thiomalic acid.

### 3.2. Antifungal activity

Considering that the GOB is not an active fungi-killed agent, an antifungal adhesion test (Landing Test as shown in Fig. 4A) was designed to test its antifungal activity. Four tablets of GO, RGO, the GOC and the GOB equidistantly adhere on the solid medium, and *M. racemosus* solution is dropped in the center of the plate. When *M. racemosus* divergently grows and slowly contacts with the materials, it can choose to bypass or adhere on the materials. After 5 days' incubation, a significant phenomenon can be observed that *M. racemosus* passes through the location of the tablets and adheres on the surface of some tablets (Fig. 4B). The RGO tablet is covered complete by *M. racemosus*, and the GO tablet and the GOC tablet are gradually covered with *M. racemosus*. The GOB tablet is the only one that no *M. racemosus* cells adhered or grew on it (Fig. 4B). Look closely to the frontier of the tablets, we can see that a large number of *M. racemosus* cells gathers in the frontier of the tablets of GO, RGO and the GOC. The edges of the tablets are ambiguous, and lots of *M. racemosus* cells climb on the surface of them (Fig. 4C). This result was consisted with the previous study that solid GO or solid RGO is no resistance to fungi [29]. They can arbitrarily propagate on the surface of these materials. In contrast, the GOB displays perfect antifungal activity. *M. racemosus* grow outside the GOB tablet. Only a few individual cells scatter in the edge of the GOB.

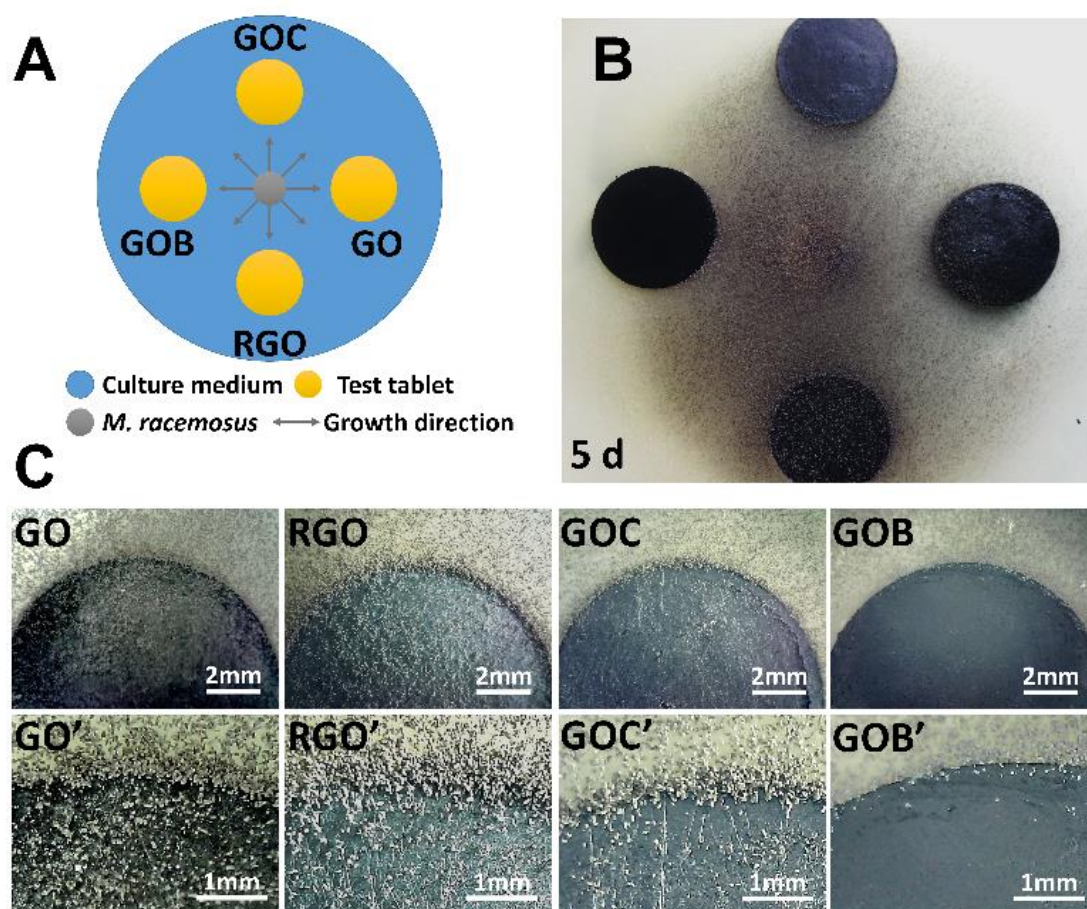


**Fig. 4.** Antifungal activity of GO, RGO, the GOC and the GOB. (A) Schematic representation of antifungal model. (B) Optical photograph of antifungal activity of the samples by culturing *M. racemosus* for 5 days. (C) Enlarged images of (B).

SEM measurements were carried out to study the morphologies of the adhered *M. racemosus* on the above-mentioned tablets. Generally, the reproduction of *M. racemosus* undergoes spherical growth and hyphae formation [57]. Once the material is capture by *M. racemosus*, there are large number of hyphae left on the surface of the material. As shown in Fig. 5, there are large numbers of grown sporangia and hyphae

adhering on the surface of GO, the GOC and especially RGO. *M. racemosus* climbs on and reproduces on the surface of these materials. The spores therein keep growth vigor as they are obviously invagination. But for the GOB, its surface is clean, and only a few hyphae are found near the boundary. The serendipitous spores are in the resting state that presents a whole sphericity. These phenomena indicated that the GOB inhibited adhesion and growth of *M. racemosus*, and thus is a powerful antifungal material.

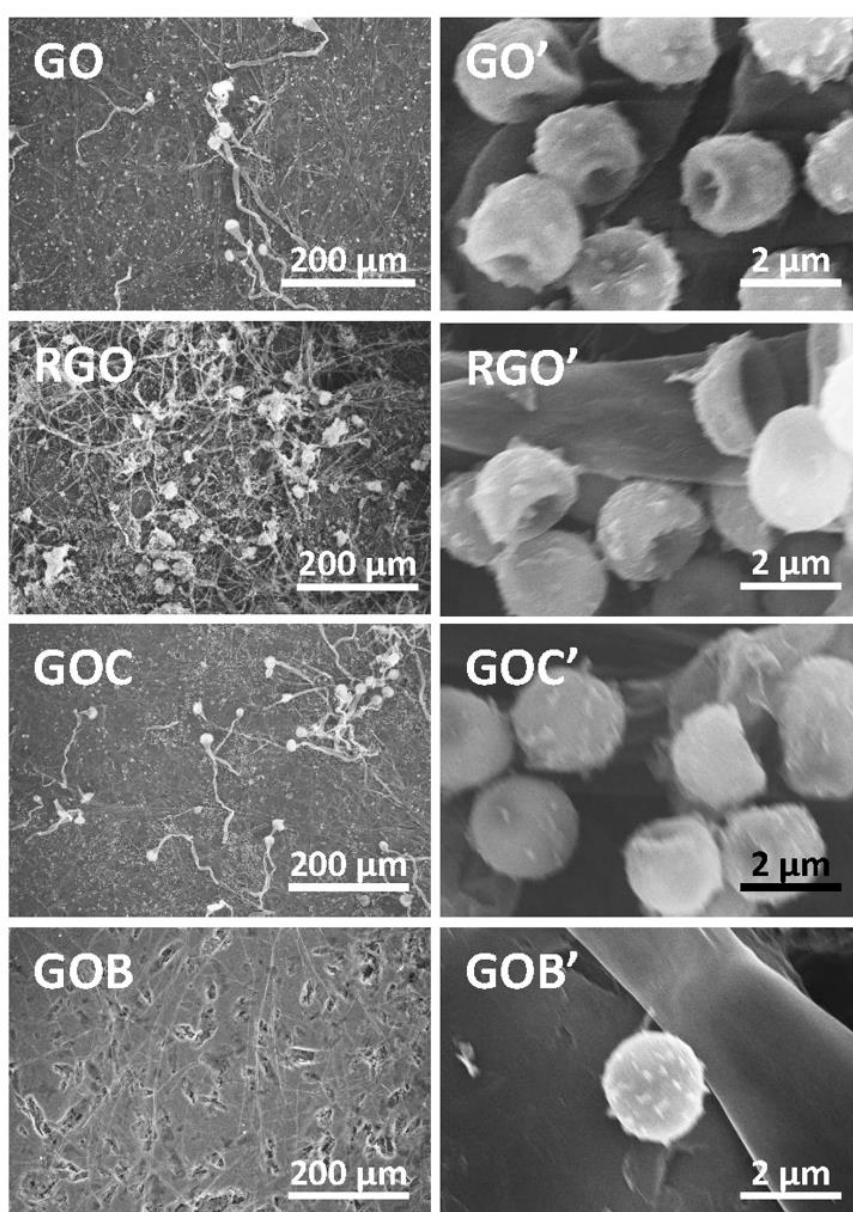


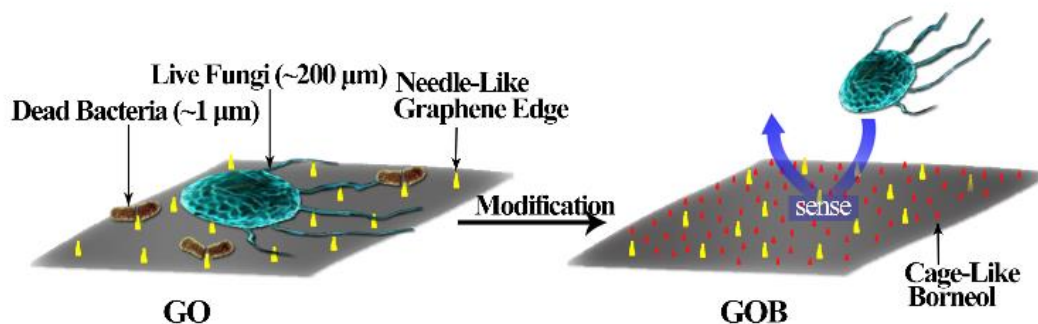
**Fig. 5.** Scanning Electron Microscope (SEM) images of antifungal adhesion results for the surface of GO, RGO, the GOC and the GOB.

### 3.3. Antifungal Mechanism

The GMs are widely studied as antimicrobial materials [6–10,15]. The recognized mechanisms mainly include nanoknives generated by the action of sharp edges, oxidative stress mediated with reactive oxygen species (ROS) production or charge transfer, and membrane wrapping or trapping derived from the flexible graphene sheet [7]. However, most of these mechanisms are set forth when the GMs are dispersed in solution. Recently, Jia *et al* revealed that needlelike nanostructure of the solid graphene surface can destroy bacterial membrane and trigger the efflux of cytoplasmic inclusion. Besides, bacterial metabolism is disturbed by ROS production and charge transfer on the surface of solid graphene [58].

However, these antibacterial mechanisms are not feasible in antifungal performance of on-surface GO or RGO (Fig. 4 and 5). Both of them have no resistance to the contamination of fungi. As one kind of filamentous fungi, *M. racemosus* contains a large member of hyphae, and these hyphae can develop from any of the spore types [57]. Thus, these hyphae like the hands of *M. racemosus* to feel and identify the surface of the materials. As shown in Fig. 5, hyphae are about 200  $\mu\text{m}$  length [57], which are much larger than bacteria (about 1-3  $\mu\text{m}$ ). Therefore, the hyphae are large enough that

they can weaken the damage caused by the needlelike nanostructure of the solid GO or the solid RGO (Scheme 2) [58].



**Scheme 2.** Schematic representation of the antifungal mechanism of the GOB. Fungi are large enough that they can weaken the damage caused by the needlelike nanostructure of the solid GO, while fungi avoid adhering on the surface of the GOB by sensing the carbon stereochemistry of the GOB.

When borneol was grafted to GO, the obtained GOB showed long-term antifungal performance. This fact was mainly due to the following reasons. First, borneol is a camphane-type bicyclic monoterpent that has complex carbon stereochemistry. It has three chiral centers within the molecular cage. Compared with the compounds contain ethylene glycol groups or hydroxyl groups, this kind of bicyclic carbon cages are correlated with lower microbial attachment [59]. Its small molecules can highly damage and disrupt fungal cell walls, and cause disappearance of cellular organelles [60]. When borneol was grafted to GO, the obtained GOB inherited the carbon stereochemistry on material surface. Microbes driving by the sensing system will avoid contacting or

adhering with this cage-like molecular structure (Scheme 2) [59]. Second, borneol is anchored on the surface of GO nanosheet by the linker (thiomalic acid). These linkers are in favor of increasing the amount and improving the distribution of borneol on the surface of the GOB. In addition, the covalent bonding between borneol and GO prevents the shedding of borneol. This physical and chemical stability prolongs the antifungal performance of the GOB. Third, because the linker is flexible, large numbers of borneol can swing freely on the surface of the rigid GOB. These flexible borneols effectively disturb the contacted *M. racemosus* on the surface of the GOB [26]. The fallen cells will also be suppressed by those surface borneol signal molecules through influencing the cell's sensing system [46]. In another word, *M. racemosus* perceive the defence on the surface of the GOB and avoid contact with the solid GOB tablet. Therefore, this strategy of surface stereochemistry is in favor of antifungal performance.

Furthermore, the effect of carbon stereochemistry is more important than that of surface wettability on the antifungal performance of the GOB. Although the WCA of RGO (99°) is higher than that of the GOB (75°), the antifungal activity of RGO is weakest (Fig. 3B). At the same time, more hydrophilic surfaces of GO (62°) and the GOC (70°) also showed no resistance to *M. racemosus*. Both of these materials could not defence the infection and adhesion of fungi on their surface, since fungi easily climbed on the surface of these materials without any obstacles. Clearly, although the wettability of the GOB is the one in the middle, the GOB is the only one that showed great antifungal performance. Therefore, it is carbon stereochemistry rather than

surface wettability endows the GOB a superb performance in inhibiting *M. racemosus* adhesion and growth on the surface.

### 3.4. Cytotoxicity Evaluation

To further confirm the biocompatibility of the GOB, MTT assay was carried out with reported method [61]. As shown in Fig. 6, the RGR of GO, the GOC and the GOB are about 80%. According to the standard toxicity rating, the cells toxicity of these materials are in grade 1, suggesting that these materials are no toxicity in the framework of safety for use. But the RGR of RGO is below 50%, presenting high cell toxicity in grade 3. This result was also in an agreement with the previous study that RGO can significantly reduce the cell viability compared with GO [17]. Overall, the GOB is non-cytotoxic and can be safely used for related applications.

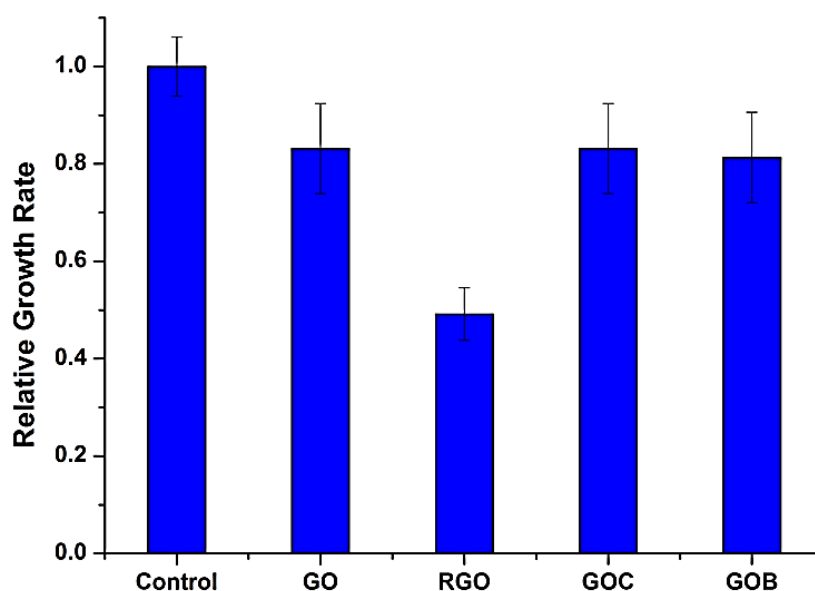


**Fig. 6.** MTT assay of GO, RGO, the GOC and the GOB. Data values corresponded to mean  $\pm$  SD (n=6).

#### **4. Conclusions**

In summary, we developed a novel graphene-based antifungal material GOB by esterification of borneol with thiomalic-acid-modified GO sheets. With a modified density of 23.8 wt% of borneol, the antifungal activity of the GOB displays a dramatically conversion from GO's affinity to distinct antifungal adhesion and growth inhibition. Deeply insight revealed that the carbon stereochemistry of the GOB was essential for this powerful antifungal performance. The covalent banding between GO and borneol molecules ensured its safe and long-term antifungal characteristic. Cytotoxicity assay also highlighted biocompatibility of the GOB. Thus, we believe that this work not only develops new strategies to control fungi adhesion, but also presents a new understanding of the GMs for advancing potential applications in antifungal fields.

#### **Acknowledgements**

The authors thank the National Natural Science Foundation of China (21574008), and the Fundamental Research Funds for Central Universities (PYBZ1709, XK1701) for their funding support.

#### **Notes and references**

- [1] C. Alberti, A. Bouakline, P. Ribaud, C. Lacroix, P. Rousselot, T. Leblanc, F. Derouin, *J. Hosp. Infect.* 48 (2001) 198–206.

- [2] E.D. Brown, G.D. Wright, *Nature* 529 (2016) 336–343.
- [3] M. Baym, T.D. Lieberman, E.D. Kelsic, R. Chait, R. Gross, I. Yelin, R. Kishony, *Science* 353 (2016) 1147–1151.
- [4] C. Traba, J.F. Liang, *J. Controlled Release* 198 (2015) 18–25.
- [5] D. Pranantyo, L.Q. Xu, E.-T. Kang, M.K. Mya, M.B. Chan-Park, *Biomacromolecules* 17 (2016) 4037–4044.
- [6] H.M. Hegab, A. ElMekawy, L. Zou, D. Mulcahy, C.P. Saint, M. Ginic-Markovic, *Carbon* 105 (2016) 362–376.
- [7] X. Zou, L. Zhang, Z. Wang, Y. Luo, *J. Am. Chem. Soc.* 138 (2016) 2064–2077.
- [8] A. Lukowiak, A. Kedziora, W. Strek, *Adv. Colloid Interface Sci.* 236 (2016) 101–112.
- [9] S. Szunerits, R. Boukherroub, *J. Mater. Chem. B* 4 (2016) 6892–6912.
- [10] J. Zhu, J. Wang, J. Hou, Y. Zhang, J. Liu, B. Van der Bruggen, *J. Mater. Chem. A* 5 (2017) 6776–6793.
- [11] X. Zhang, J. Yin, C. Peng, W. Hu, Z. Zhu, W. Li, C. Fan, Q. Huang, *Carbon* 49 (2011) 986–995.
- [12] X. Zhang, W. Hu, J. Li, L. Tao, Y. Wei, *Toxicol. Res.* 1 (2012) 62–68.
- [13] Y. Shi, M. Liu, K. Wang, F. Deng, Q. Wan, Q. Huang, L. Fu, X. Zhang, Y. Wei, *Polym. Chem.* 6 (2015) 5876–5883.
- [14] M. Liu, G. Zeng, K. Wang, Q. Wan, L. Tao, X. Zhang, Y. Wei, *Nanoscale* 8 (2016) 16819–16840.

- [15] H. Ji, H. Sun, X. Qu, *Adv. Drug Delivery Rev.* 105 Part B (2016) 176–189.
- [16] S. Chen, L. Yuan, Q. Li, J. Li, X. Zhu, Y. Jiang, O. Sha, X. Yang, J. Xin, J. Wang, F.J. Stadler, P. Huang, *Small* 12 (2016) 3516–3521.
- [17] W. Hu, C. Peng, W. Luo, M. Lv, X. Li, D. Li, Q. Huang, C.H. Fan, *ACS Nano* 4 (2010) 4317–4323.
- [18] S. Liu, T. Zeng, M. Hofmann, E. Burcombe, J. Wei, R. Jiang, J. Kong, Y. Chen, *ACS Nano* 5 (2011) 6971–6980.
- [19] Y. Tu, M. Lv, P. Xiu, T. Huynh, M. Zhang, M. Castelli, Z. Liu, Q. Huang, C. Fan, H. Fang, R. Zhou, *Nat. Nanotechnol.* 8 (2013) 594–601.
- [20] L. Hui, J.-G. Piao, J. Auletta, K. Hu, Y. Zhu, T. Meyer, H. Liu, L. Yang, *ACS Appl. Mater. Interfaces* 6 (2014) 13183–13190.
- [21] X. Ye, J. Feng, J. Zhang, X. Yang, X. Liao, Q. Shi, S. Tan, *Colloids Surf. B Biointerfaces* 149 (2017) 322–329.
- [22] A. Biswas, P. Khandelwal, R. Das, G. Salunke, A. Alam, S. Ghorai, S. Chattopadhyay, P. Poddar, *J. Mater. Chem. B* 5 (2017) 785–796.
- [23] J. Chen, X. Zhang, H. Cai, Z. Chen, T. Wang, L. Jia, J. Wang, Q. Wan, X. Pei, *Colloids Surf. B Biointerfaces* 147 (2016) 397–407.
- [24] Q. Tu, C. Tian, T. Ma, L. Pang, J. Wang, *Colloids Surf. B Biointerfaces* 141 (2016) 196–205.

- [25] A.F. de Faria, D.S.T. Martinez, S.M.M. Meira, A.C.M. de Moraes, A. Brandelli, A.G. Souza Filho, O.L. Alves, *Colloids Surf. B Biointerfaces* 113 (2014) 115–124.
- [26] B.R. Coad, S.E. Kidd, D.H. Ellis, H.J. Griesser, *Biotechnol. Adv.* 32 (2014) 296–307.
- [27] J. Wu, Y. Zheng, X. Wen, Q. Lin, X. Chen, Z. Wu, *Biomed. Mater.* 9 (2014) 035005.
- [28] L. Chen, J.F. Liang, *Biomacromolecules* 14 (2013) 2326–2331.
- [29] X. Dai, Q. Guo, Y. Zhao, P. Zhang, T. Zhang, X. Zhang, C. Li, *ACS Appl. Mater. Interfaces* 8 (2016) 25798–25807.
- [30] C. Li, X. Wang, F. Chen, C. Zhang, X. Zhi, K. Wang, D. Cui, *Biomaterials* 34 (2013) 3882–3890.
- [31] J. Chen, L. Sun, Y. Cheng, Z. Lu, K. Shao, T. Li, C. Hu, H. Han, *ACS Appl. Mater. Interfaces* 8 (2016) 24057–24070.
- [32] J. Chen, H. Peng, X. Wang, F. Shao, Z. Yuan, H. Han, *Nanoscale* 6 (2014) 1879–1889.
- [33] S. Arora, J. Jain, J.M. Rajwade, K.M. Paknikar, *Toxicol. Lett.* 179 (2008) 93–100.
- [34] S. Arora, J. Jain, J.M. Rajwade, K.M. Paknikar, *Toxicol. Appl. Pharmacol.* 236 (2009) 310–318.
- [35] L. Rizzello, P.P. Pompa, *Chem. Soc. Rev.* 43 (2014) 1501–1518.

- [36] R.P. Tengerdy, Trends Biotechnol. 3 (1985) 96–99.
- [37] T.T. Sein, R. Spurio, C. Cecchini, A. Cresci, Int. Biodeterior. Biodegrad. 63 (2009) 901–905.
- [38] C. Alberti, A. Bouakline, P. Ribaud, C. Lacroix, P. Rousselot, T. Leblanc, F. Derouin, J. Hosp. Infect. 48 (2001) 198–206.
- [39] X. Wang, H. Gan, T. Sun, B. Su, H. Fuchs, D. Vestweber, S. Butz, Soft Matter 6 (2010) 3851–3855.
- [40] X. Wang, H. Gan, T. Sun, Adv. Funct. Mater. 21 (2011) 3276–3281.
- [41] X. Wang, H. Gan, M. Zhang, T. Sun, Langmuir 28 (2012) 2791–2798.
- [42] J. El-Gindi, K. Benson, L. De Cola, H.-J. Galla, N.S. Kehr, Angew. Chem. Int. Edit. 51 (2012) 3716–3720.
- [43] D. Bandyopadhyay, D. Prashar, Y.-Y. Luk, Chem. Commun. 47 (2011) 6165–6167.
- [44] S.Y. Lee, S.H. Kim, C.Y. Hong, M.J. Park, I.G. Choi, Flavour Fragrance J. 28 (2013) 129–134.
- [45] R.E. Granger, E.L. Campbell, G.A.R. Johnston, Biochem. Pharmacol. 69 (2005) 1101–1111.
- [46] L. Luo, G. Li, D. Luan, Q. Yuan, Y. Wei, X. Wang, ACS Appl. Mater. Interfaces 6 (2014) 19371–19377.
- [47] X. Sun, Z. Qian, L. Luo, Q. Yuan, X. Guo, L. Tao, Y. Wei, X. Wang, ACS Appl. Mater. Interfaces 8 (2016) 28522–28528.

- [48] B. Shi, D. Luan, S. Wang, L. Zhao, L. Tao, Q. Yuan, X. Wang, *RSC Adv.* 5 (2015) 51947–51952.
- [49] W.S. Hummers, R.E. Offeman, *J. Am. Chem. Soc.* 80 (1958) 1339–1339.
- [50] G. Li, X. Wang, L. Tao, Y. Li, K. Quan, Y. Wei, L. Chi, Q. Yuan, *J. Membr. Sci.* 495 (2015) 439–444.
- [51] D. Chen, H. Feng, J. Li, *Chem. Rev.* 112 (2012) 6027–6053.
- [52] O.C. Compton, S.T. Nguyen, *Small* 6 (2010) 711–723.
- [53] H. Hu, Z. Zhao, W. Wan, Y.J. Gogotsi, Qiu, *Adv. Mater.* 25 (2013) 2219–2223.
- [54] W. Shao, X. Liu, H. Min, G. Dong, Q. Feng, S. Zuo, *ACS Appl. Mater. Interfaces* 7 (2015) 6966–6973.
- [55] A.C. Ferrari, J.C. Meyer, V. Scardaci, C. Casiraghi, M. Lazzeri, F. Mauri, S. Piscanec, D. Jiang, K.S. Novoselov, S. Roth, A.K. Geim, *Phys. Rev. Lett.* 97 (2006) 187401.
- [56] O. Akhavan, *Carbon* 81 (2015) 158–166.
- [57] M. Orlowski, *Microbiol. Rev.* 55 (1991) 234–258.
- [58] Z. Jia, Y. Shi, P. Xiong, W. Zhou, Y. Cheng, Y. Zheng, T. Xi, S. Wei, *ACS Appl. Mater. Interfaces* 8 (2016) 17151–17165.
- [59] A.L. Hook, C.-Y. Chang, J. Yang, J. Lockett, A. Cockayne, S. Atkinson, Y. Mei, R. Bayston, D.J. Irvine, R. Langer, D.G. Anderson, P. Williams, M.C. Davies, M.R. Alexander, *Nat. Biotechnol.* 30 (2012) 868–875.

- [60] S.Y. Lee, S.H. Kim, C.Y. Hong, M.J. Park, I.G. Choi, *Flavour Frag. J.* 28 (2013) 129–134.
- [61] K. Quan, G. Li, D. Luan, Q. Yuan, L. Tao, X. Wang, *Colloids Surf., B Biointerfaces* 132 (2015) 27–33.